*SACLANT UNDERSEA
RESEARCH CENTRE
MEMORANDUM*

BOTTOM SCATTERING MEASUREMENTS IN SHALLOW WATER

C.W. Holland, R. Hollett, L. Troiano

August 1999

The SACLANT Undersea Research Centre provides the Supreme Allied Commander Atlantic (SACLANT) with scientific and technical assistance under the terms of its NATO charter, which entered into force on 1 February 1963. Without prejudice to this main task – and under the policy direction of SACLANT – the Centre also renders scientific and technical assistance to the individual NATO nations.

This document is approved for public release.
Distribution is unlimited

SACLANT Undersea Research Centre
Viale San Bartolomeo 400
19138 San Bartolomeo (SP), Italy

tel: +39-0187-5271
fax: +39-0187-527.420

e-mail: library@saclantc.nato.int

NORTH ATLANTIC TREATY ORGANIZATION

SACLANTCEN SM-364

.

.

Bottom scattering measurements in shallow water

Holland, C.W., Hollett, R., Troiano, L.

Jan L. Spoelstra
Director

intentionally blank page

SACLANTCEN SM-364

Bottom scattering measurements in shallow water

Holland, C.W., Hollett, R., Troiano, L.

Executive Summary: Sonar performance predictions of reverberation in shallow water rely upon good estimates of the bottom scattering strength and reverberation statistics. This report describes a new technique for measuring bottom scattering in shallow water. The technique employs a vertical receive array, with either broadband incoherent sources (lightbulbs) or coherent sources. Five coherent sources were designed with a spacing to minimize multipaths at 600, 1200 Hz, 1800 Hz and 3600 Hz. The technique is not only capable of producing scattering strengths (both monostatic and vertically bi-static) but can also provide direct evidence of the bottom scatter mechanism (current modeling techniques have to rely on sometimes tenuous clues for discerning the bottom scatter mechanism). This feature of the measurement technique is particularly important, inasmuch as determining the physical scattering mechanism is crucial for eventual database development in support of low frequency active sonar performance predictions. There is also mounting evidence that the second-order reverberation statistics (i.e., clutter) can be linked to the bottom scatter mechanism. Bottom scatter measurements and interpretations are provided at two shallow water sites in the Ligurian Sea. The results show that the measurement technique is viable, and shows the surprising result that sub-bottom scattering from as deep as 25 m in the sediments can contribute to the scattering at 1800 Hz.

intentionally blank page

SACLANTCEN SM-364

Bottom scattering measurements in shallow water

Holland, C.W., Hollett, R., Troiano, L.

Abstract: Sonar performance predictions of reverberation in shallow water rely upon good estimates of the bottom scattering strength. However, little is understood about bottom scattering in shallow water in the frequency range 400 – 4000 Hz, particularly its dependency upon frequency and its relationship to the physical properties of the seafloor. In order to address these issues, new measurement techniques have been developed to probe the frequency and angular dependency of bottom scattering strength. The measurement techniques also appear to be capable of revealing the physical mechanisms that give rise to the scattering. Several experimental techniques will be described, including use of coherent and incoherent sources (lightbulbs). The general experimental approach is also described which includes auxiliary acoustic and geoacoustic measurements designed to allow exploration of the relationship between bottom scattering and the physical properties of the bottom. Measurement and modeling results for two shallow water sites are presented. At one site, the scattering appeared to arise from at or near the water-sediment interface. At the other site, scattering from a 25 m sub-bottom horizon is clearly apparent in the data at and below 1800 Hz.

Keywords:

Contents

1

Introduction

The traditional method for estimating bottom scattering strength in shallow water is by measuring long range reverberation, and extracting the scattering strength via modeling. A few examples in the frequency range of interest of this study include Urick (1970), Cole and Podeswa (1974), Blanc *et al.* (1978), Zhou *et al.* (1983), Ellis (1995), Scanlon *et al.*(1996), and Cable *et al.* (1997). The advantages of this method are that the measurements are easy to conduct and that the scattering strength is averaged over a large spatial area. The disadvantage of the method is that the scattering strength estimate is subject to a rather large set of assumptions[1]. A significant assumption pertains to the incident field at the seafloor. Frequently it is not measured, e.g., Blanc *et al.* (1978) assume a perfectly reflecting bottom. Sometimes transmission loss (TL) is measured in the water column, however, this does not guarantee the correct modeling of the incident field at the seafloor, which depends upon knowing the geoacoustic properties. Since reverberation can be dominated much more by the propagation than by the scattering events, it is inherently difficult to extract scattering information without knowledge about the propagation. Moreover, it is almost universally assumed that the scattering mechanism is at the water sediment interface. Other common assumptions include range and azimuthal independence in TL and/or scattering strength and assumptions about the absence or presence of air-sea interface and biologic scattering. It is worth noting that the reported frequency dependence of the scattering strength can be an artifact of any of these assumptions. Thus, the ability to probe the frequency dependence of shallow water bottom scattering using long range reverberation data may be limited.

An alternative approach is to make direct path measurements of bottom scattering. The disadvantage of this type of measurement in shallow water is the presence of multipaths, which makes it difficult to isolate specific paths of interest. Another disadvantage is that the measurement only samples a very small region, which may not be immediately useful for making reverberation predictions over large regions. However, the principal advantage of the direct path measurement technique is that many of the assumptions that plague interpretation of the reverberation data are eliminated, so that the frequency and angular dependence of bottom scatter can be studied in detail. Thus, the direct path measurements might also serve as a basis from which to examine the validity of the assumptions commonly applied to extract scattering strength from reverberation measurements. Another important advantage of the direct path technique is the potential for revealing the dominant scattering mechanisms in a particular environment, i.e., for discerning the relative contributions of water-sediment interface, sub-bottom volume or sub-bottom horizon scattering.

---

[1] In addition to the disadvantages posed by the following assumptions, the method is not well suited for probing the angular dependence of bottom scattering.

The scope of this paper is to describe the direct path bottom scatter measurement technique, show measurements in two diverse sedimentary regimes, and present some initial interpretation. The Capraia Basin (see Fig. 1), was selected as the study area because of its diversity in bottom types including flat thickly sedimented regions, and magmatic rock outcrops.
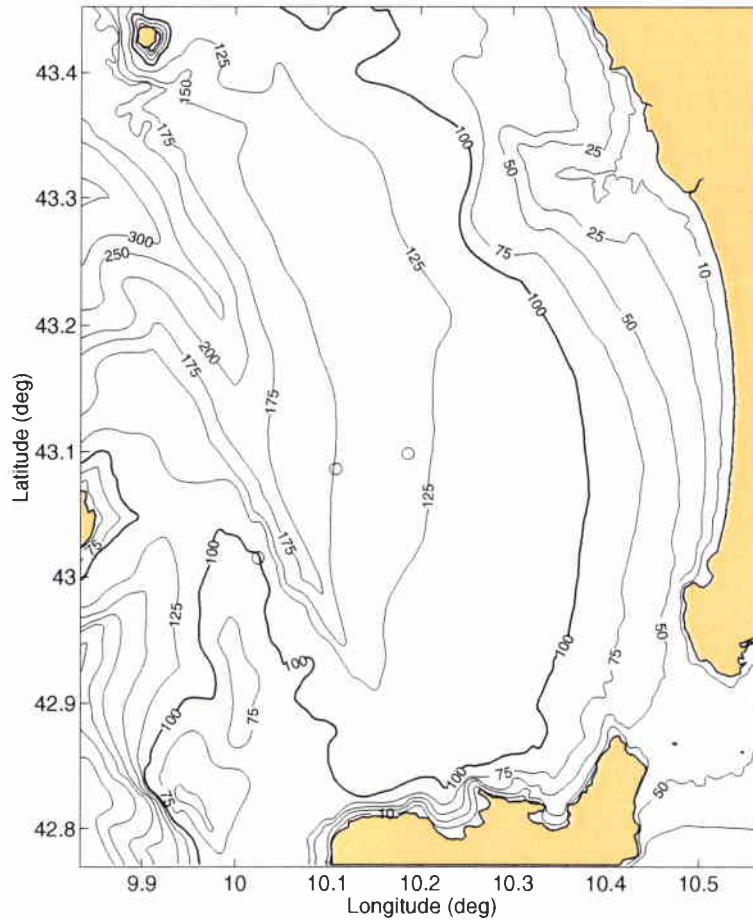
Figure 1 *Experiment area showing locations (o) of bottom scatter measurements. Measurement locations are designated from east to west as Site 1, Site 2, and Site 3.*

SACLANTCEN SM-364

2

Experiment design

The experimental design was dictated by the requirement to conduct the measurements in shallow water (water depths of 50-200 m), over a large bandwidth (400 – 4000 Hz) with greatest interest on low to intermediate grazing angles (0-45°) that control sonar system performance.

Perhaps the most significant challenges of such an experiment in shallow water is to avoid or control multipaths. One multipath problem is potential contamination by sub-bottom reflections. It is well-known that scattering may arise from not only the interface but also from sub-bottom inhomogeneities or horizons. However, sub-bottom reflections at normal incidence contaminate the scattering measurement, since the normal incidence reflections are often higher amplitude than the scattering events.

A second multipath problem is contamination from hybrid paths. Hybrid paths are paths that belong to a different family of scattering event that arrive at the same time as the scattering path that is being measured. Figures 2 and 3 show the various paths, and their relationship in time and angle. For example, in this geometry, beyond about 0.4 seconds, the monostatic (path a) and bi-static[1] paths (b, c and d) can not be separated in time or angle. A receive and/or source array with vertical aperture can be used to control both types of multipaths, i.e., by reducing the contribution of the normal incidence reflections and also providing discrimination against the various scattering paths. Short pulse lengths are required in order to resolve angular dependence of the scattering function.

---

[1] i.e., the incident and scattered angles are different in the vertical plane.
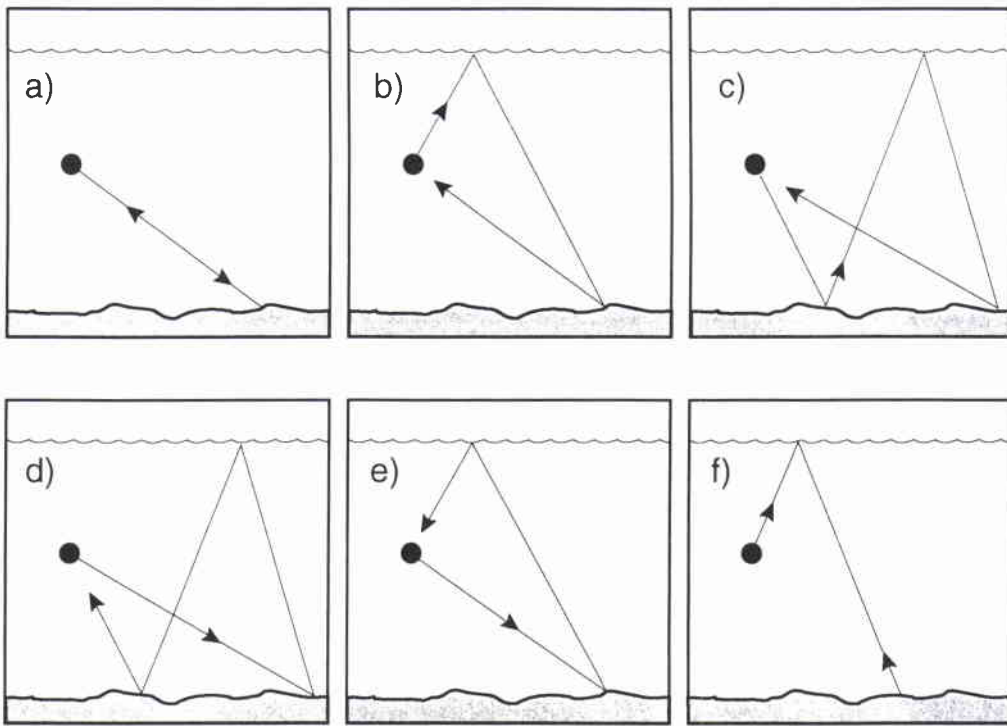
Figure 2 *Bottom scattering multi-paths. Only those paths that have less than two surface interactions are depicted.*
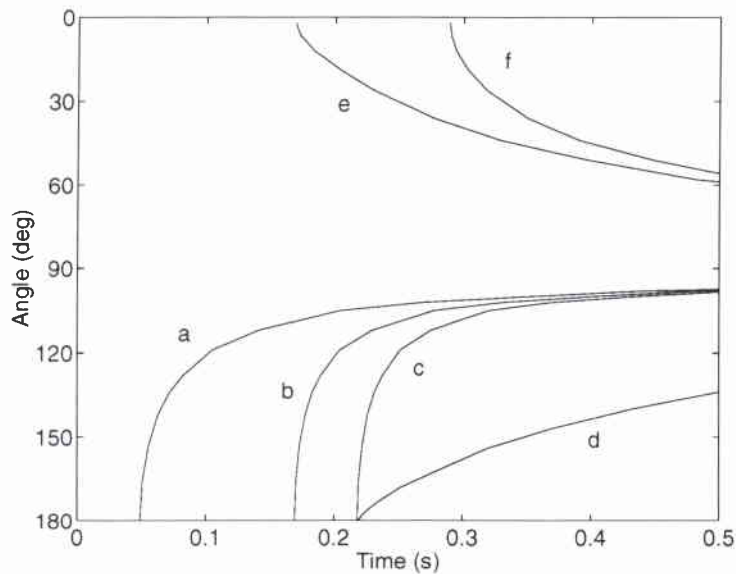
Figure 3 *Vertical arrival angles versus time for various bottom scattering paths. Source-receiver depth is 91 m and the water depth is 128 m. Time is referenced to source initiation. Angles are measured with 0 degrees towards the sea surface. Path (a) is the monostatic backscattering path. See Fig. 2 for other path descriptions.*

Figure 4 depicts the system employed in this study. The vertical aperture of the receive array helps minimize effects of multipath, in addition it provides the potential for identification of scattering mechanisms (see Section III). Two kinds of sources were employed. Short pulses from sources located near the bottom of the array provided repeatable and stable source. In addition, standard 100 W lightbulbs were employed as an inexpensive and safe broadband pulses. The equipment is deployed from the forecastle and the ship is either set in a single point moor or left to drift. The weight of the Mod-40s (90 kg in water) provides enough ballast to keep the array straight when the current shear is small. A small fin (not shown) on the Mod40 frame stabilizes the array from rotational forces. The source-receive array was placed at various heights above the seafloor in order to explore the potential for inferring sub-bottom scattering from diversity in source heights.
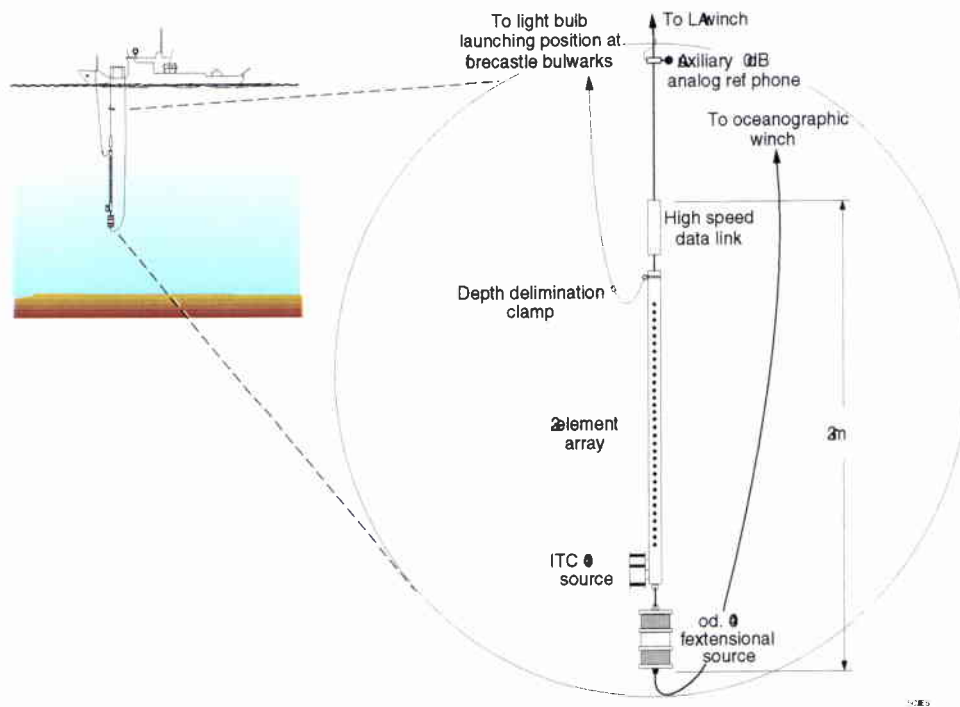
Figure 4 *Experiment geometry used for measuring bottom scattering. Details of the source and receive arrays are found in the text.*

In addition to the direct path bottom scattering measurements, associated acoustic and geophysical measurements were conducted. The purpose of these measurements was to provide the environmental basis to understand the relationship between the scattering and the physical properties of the sediment. Shallow water bottom loss measurements (Holland and Osler (1999)) were designed to provide high resolution (of order 50 cm in the vertical plane) sub-bottom deterministic properties. Core data provided additional

sound speed and density data in the upper 5 m   Seismic reflection and SWATH bathymetry data provided regional understanding of sub-bottom layering structure and water-sediment interface morphology.

2.1 Coherent sources

Modeling indicated that for some environments (large reflection coefficients at normal incidence relative to the scattering) directivity in both the source and receiver is required in order to control bottom and sub-bottom reflections.   Thus a source array was constructed with pairs at $\lambda/2$ spacing in the vertical so that transmitting in-phase would yield a theoretical null on the vertical axis (see Fig. 5). The mid-frequency source array was constructed of 3 ITC-4001 transducers spaced at 18 cm and 42 cm, to yield $\lambda/2$ spacing at 3600 Hz, 1800 Hz, and 1200 Hz. The top of this array was placed 1 m below the bottom phone of the receive array. The low frequency array consisted of 2 Mod 40 flextensional transducers spaced at 1.25 m (or $\lambda/2$ spacing at 600 Hz). Source array calibration techniques and results are provided in Annex A.

Ping types included both CW and LFM pulses of 15 ms pulse length. Repetition rates of 6 pings/minute were used, and the acquisition system was triggered 1 second before transmit to acquire ambient noise for each ping. Ten to fifteen pings were collected for each source/receiver depth.
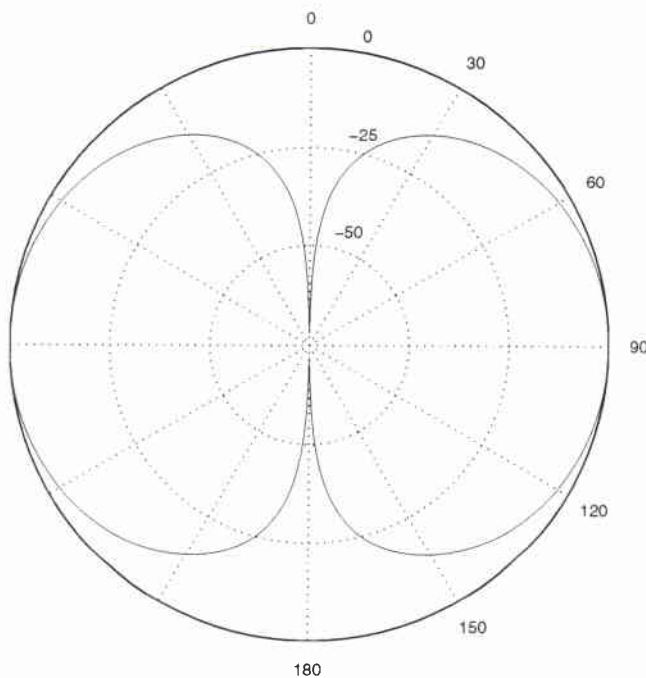
Figure 5 *Theoretical beampattern from two sources spaced at $\lambda/2$, which is symmetric around the vertical axis.*

2.2 Lightbulb sources

The acoustic signal from an ordinary lightbulb that is imploded can make a useful source for undersea experiments (see Heard *et al.* (1997)) for a good review of the subject). The signal is generated from oscillations of the gas bubble that is released after the implosion. The advantage of the lightbulbs as acoustic sources is their low cost and safety relative to explosives if a high source level is not required. Another advantage is their short time signature - on the order of 5 milliseconds at 100 m depth. While lightbulbs and laboratory glassware have been used by other researchers for various purposes this is the first time to the author's knowledge that they have been used for bottom scattering strength measurements.

The nominal crush depth for a typical lightbulb is about 270 m The experiment concept required that implosion depth be easily controlled from depths of 20-150 m This was accomplished by attaching the lightbulb to a 4 kg weight which was designed to slide freely down a kevlar rope attached to the top of the receive array. A depth delimitation ring placed on the wire 1.5 m above the top of the receive array served as the crush plate. Rubber padding on the bottom of the weight minimized a secondary acoustic signal arising from the weight striking the crush plate.

Figure 6 shows a lightbulb source signal at about 90 m depth. The acoustic pressure is about 180° out of phase with the bubble displacement. Thus, the pressure peaks occur when the bubble is at its smallest radius. Five or six acoustic peaks are visible before the potential energy of the gas bubble is dissipated (see McDonald and Holland (1999)) for a model of bubble pulse decay characteristics).
Figure 7 shows the source level for three consecutive shots at the same depth. The undulating behavior of the source level at the low frequencies arises from constructive and destructive interference between the bubble pulses. One of the shots was audibly different from the others and possibly was misaligned on the rope when it struck the crush plate. For this shot the second bubble pulse was much lower than the others. Thus, a disadvantage of lightbulb sources is the variability in source signature that requires measurement of each implosion.

Preparation time required for each lightbulb deployment gave an implosion rate of typically 1 implosion every 4 minutes. The triggering was done manually using the observed 2 m/s fall rate of the weight and lightbulb assembly.
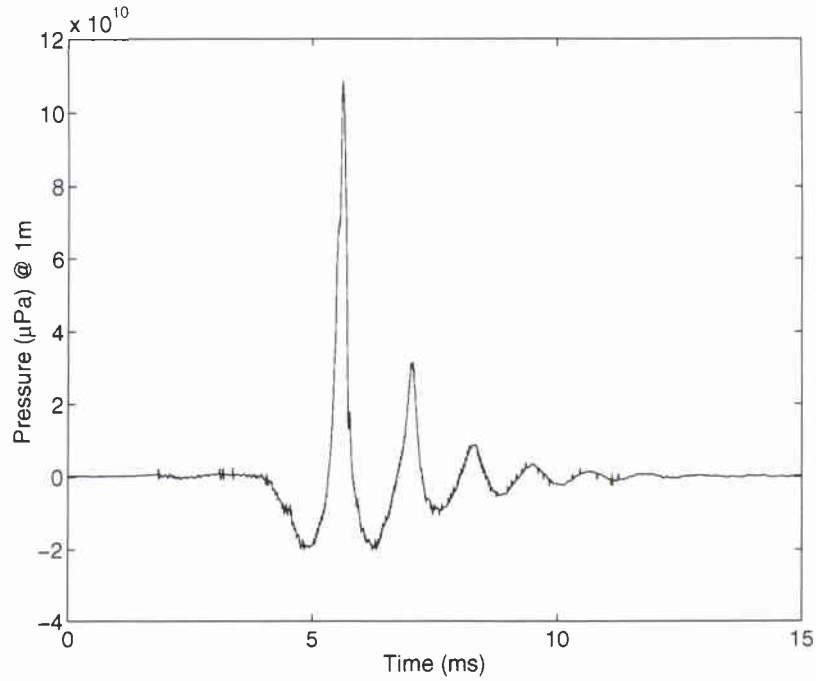
Figure 6 *Lightbulb implosion at about 90 m depth corrected to 1m.*
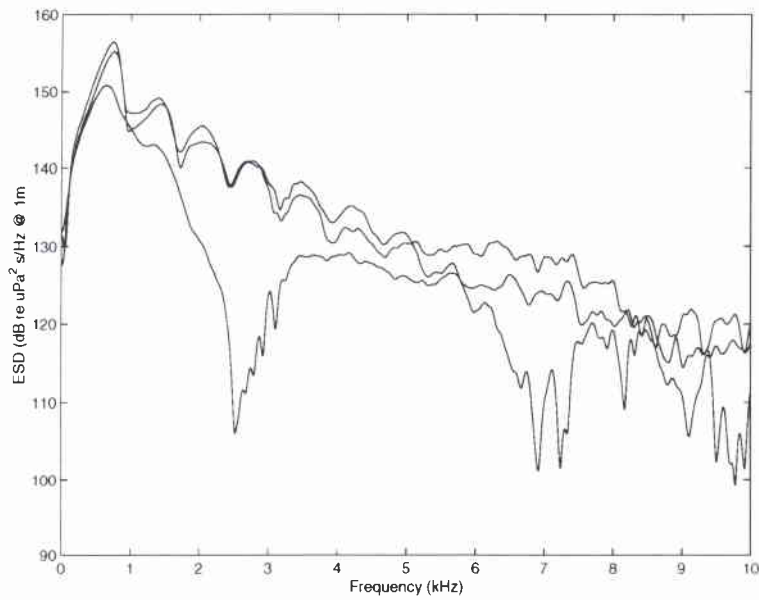
Figure 7 *Source level (energy spectral density) for three successive implosions at 90m depth. The variability in source signature requires measurement of each bulb implosion.*

SACLANTCEN SM-364

2.3 Receiver

The receive array consisted of 32 Benthos AQ-4 hydrophones with a 0.18 m spacing. The data were sampled at 12 kHz and low pass filtered at 3.8 kHz with a seven-pole six-zero elliptic (70 dB per octave roll off) anti-alias filter. The RC high pass filter (6 dB per octave roll off) was set at 150 Hz. A high speed digital link within the array provided programmable signal conditioning, digitization and serialization of the signals . The array was hardwired directly to the NATO Research Vessel (NRV) *Alliance*. Non acoustic data (gains, filter settings, etc.) were interleaved in the serial stream.

A separate reference hydrophone, 14 m above the crush plate, was employed in order to acquire the data at a higher sampling rate (50 kHz) which was necessary for studying the details of the lightbulb source characteristics. A separate reference hydrophone was also required because the dynamic range of the vertical array was insufficient for acquiring both the direct blast and the scattered field

3

Data processing

Data processing details are presented for several types of processed outputs. The simplest processing is a display of the filtered, beam formed results. These data can then be further processed to produce bottom scattering strengths.

3.1 Beam time series

Following signal conditioning, data were beamformed (Hanning shading) using a plane wave time domain beamformer (see Sylva *et al.* (1986)) implemented in hardware. Beams were spaced to yield 3 dB down crossing points at the design frequency of the array (see Table 1). The data are filtered with a 6th order lowpass digital elliptic filter with 0.5 decibels of ripple in the passband and a stopband 50 dB down. Bandwidths were chosen to be 150 Hz.

Table 1. *Receive array steer angles corresponding to beam numbers*

Beam	1	2	3	4	5	6	7	8	9	10	11	12
Angle	2.1	24.7	35.2	43.4	50.5	57.0	63.0	68.7	74.2	79.5	84.8	90.0
Beam	13	14	15	16	17	18	19	20	21	22	23	'24
Angle	95.2	100.5	105.8	111.3	117.	123.	129.5	136.6	144.8	155.3	177.9	180

The far field was estimated as d^2/λ, where λ is acoustic wavelength and d is the effective array length[1] as shown in Fig. 8. Thus, the experiments were generally conducted with source/receiver heights greater than 20 m

Experimental results from a single ITC source transmitting at 3600 Hz are shown in Fig. 9. The water depth and source depth are 128 m and 91 m respectively. Zero time in the figure corresponds to the direct blast, which overloads the array and is seen on all beams. The surface reflection is visible at 0.1 sec. Also shown are the theoretical results of arrival time vs beam in the white lines which correspond to the various monostatic and bi-static scattering paths as shown in Figs. 2 and 3.

---

[1] i.e., the length of the array with shading coefficients greater than .5, which in this case is 3.06 meters.

SACLANTCEN SM-364
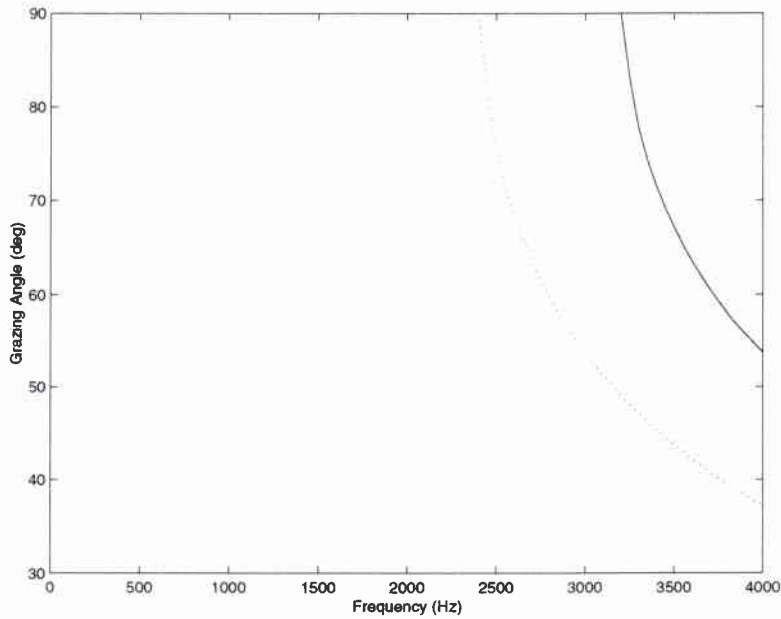
Figure 8. *Far field calculations for the array used in the bottom scatter experiment for a source height above the bottom of: 15 m (dashed) and 20 m (solid).*
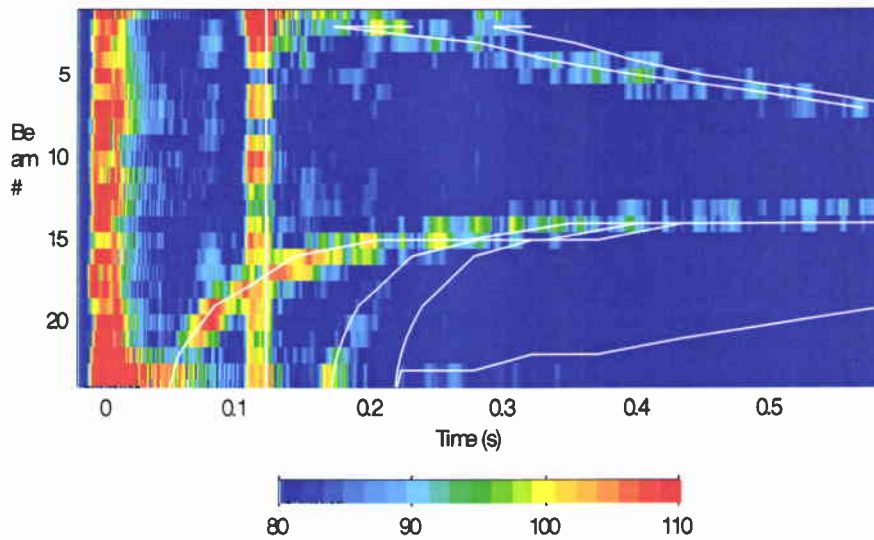
Figure 9 *Measured beam time series at Site 1, the units are dB re 1 μPa²/s/Hz. The water depth and source depth are 128 m and 91 m respectively. Predictions of multipath structure are overlaid (white lines) on the data and correspond to the paths shown in Figures 2 and 3.*

– 11 –

These data are expected to be useful for exploring the relationship between the monostatic and bistatic scattering and the sediment geoacoustic properties. They may also be useful for directly determining the scattering mechanism. That is, sub-bottom scattering will be observed as a broadening in beam space (toward higher angles) of a particular scattering branch. In practice, the ability to observe this will be limited by the pulse length (the 15 ms used in this study means that interface and sub-bottom scattering in the upper 10 ms can not be distinguished) and also by the receive array aperture. Sub-bottom volume scattering is expected to become more prominent at lower frequencies, however, at the same time the broadening of the beams leads to a reduced discrimination capability. Despite these limitations, it will be shown that the technique is capable of directly discerning the presence of sub-bottom scattering. This is an important result because up to the present, bottom scattering analyses have inferred the presence/absence of sub-bottom scattering based on the frequency and/or angular dependence of the data or deductions made about the environments rather than on direct evidence in the data (e.g., see Mourad and Jackson (1996), Novarini and Caruthers (1998), and Holland and Neumann (1998)).

3.2 Scattering strength from coherent pulses

The data of Fig. 9 can be processed for both monostatic and vertically bi-static scattering strength. In this paper the monostatic processing technique is demonstrated. For a lossless isovelocity medium, the instantaneous intensity i_o received from a scattering area can be written as:

$$i_o = \iint i \, s \, b \, b' \, r^{-4} \rho \, d\rho \, d\vartheta \tag{1}$$

where i is the transmit intensity, s is the scattering cross section, b and b' are the transmit and receive beampatterns, r is the distance from the array to the scattering patch and ρ and θ are the radial and azimuthal polar coordinates (see Fig. 10). If the beampattern is invariant over the insonified area, then:

$$s = i_o \left(b \, b' \, 8\pi \int i \, dt \right)^{-1} c^2 t^3 \left(1 - \tau/2t\right)^2 \left(1 + \tau/2t\right)^2 \tag{2}$$

When the pulse length is short $(\tau \ll 2t)$, the last two terms of Eq. (2) can be ignored yielding an expression identical to Chapman and Harris (1962).

The above assumptions are appropriate for the experimental results presented here; the frequencies are low enough and ranges short enough so that seawater absorption is negligible, the beam pattern is slowly varying with vertical angle and independent of

SACLANTCEN SM-364

azimuth, and the sound speed profiles are roughly isovelocity[1] within 30 m of the seafloor (see Fig. 11). The geometry is nearly monostatic with vertical offset between the center of the receive array and the ITC and Mod40 sources of 4 and 8 m respectively. These offsets were small enough so that in the processing, the monostatic source/receiver depth was referenced to the average depth of the source-receiver pair (see Annex B).

The only assumption which may not be met is that pertaining to the scattering process. For some environments, scattering from the sub-bottom is expected to dominate the response rather than scattering from the interface. The effect of sub-bottom scattering can either be taken into account in the processing or the subsequent modeling. Since the frequencies and environments at which sub-bottom scattering dominates are not known *a priori* we choose to process the data as if the scattering process were arising from the interface and account for any sub-bottom contributions in the modeling.
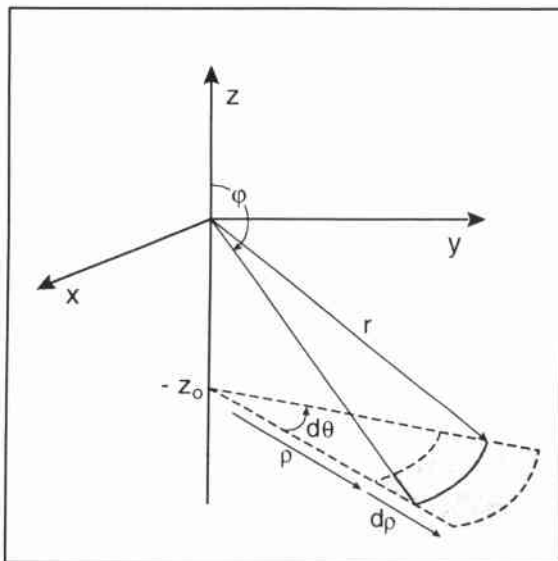
Figure 10 *Coordinate system for bottom scattering experiment.*

---

[1] The sound velocity profile effects both the TL and the mapping of time to angle. The difference between the TL from the measured profiles and that used in Eqs 1 (r^{-4}) is negligible. The mapping of time to angle is done via eigenray analysis for each profile.
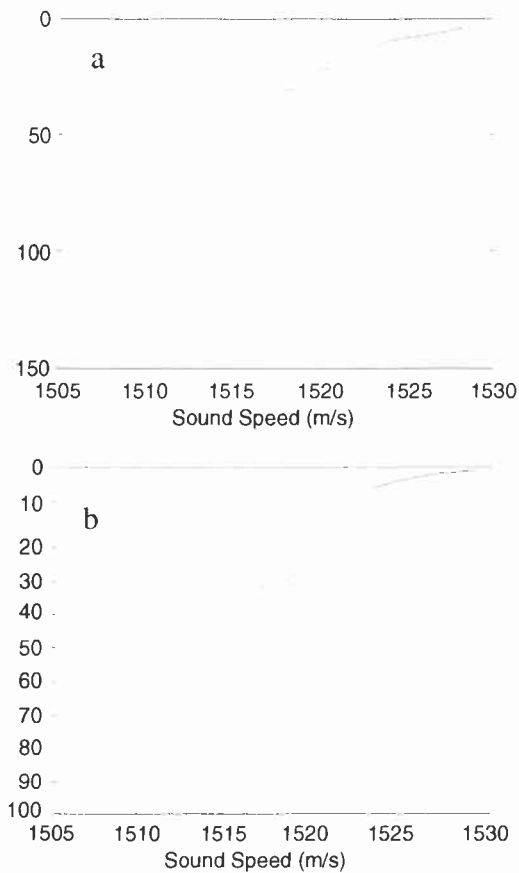
Figure 11 *Sound speed profile from CTD casts at: a) Site 2, and b) Site 3.*

The potential presence of sub-bottom contributions presents a practical problem of how to select the beams that contribute to the scattering strength at a given time. This was done in the following way. First, the peak arrivals as a function of beam and time are found along the monostatic branch, aided by using the theoretical results of arrival time vs beam as a starting solution. Then adjacent beams are summed if they fall within a certain threshold. The threshold used in the following examples was 10 dB. This choice of threshold in practice provided a useful criterion to discriminate against sub-bottom reflections and bi-static paths at early times without discarding potential contributions from neighboring beams. At late times, the bi-static paths merge with the mono-static path in beam-time space, and a measurement of backscattering strength becomes impossible unless the bi-static contributions are weak relative to the monostatic path.

Averaging was performed over several (typically 10) pings. It is more convenient to perform the averaging on the received level data rather than the scattering strength. This is possible since the experiment geometry and the source function are constant from ping-to ping. The signal-to-noise ratio (SNR) criterion was 6 dB for both the instantaneous received level and a smoothed (30 ms sliding window) average.

3.3 Scattering strength from lightbulb implosions

Scattering strength processing from the lightbulb sources was similar to that from the coherent pulses (i.e.. Eq. (2) without the last two terms). However. the sometimes significant variability in source spectrum. necessitated processing source energy flux density for each implosion as well as requiring every implosion to be fully processed to a scattering strength before averaging. Another step required in the lightbulb processing was the manual picking of the direct and surface arrivals in order to measure the implosion time and depth. Figure 12 shows an example of the data (Hilbert transform from a single phone) employed in this step.
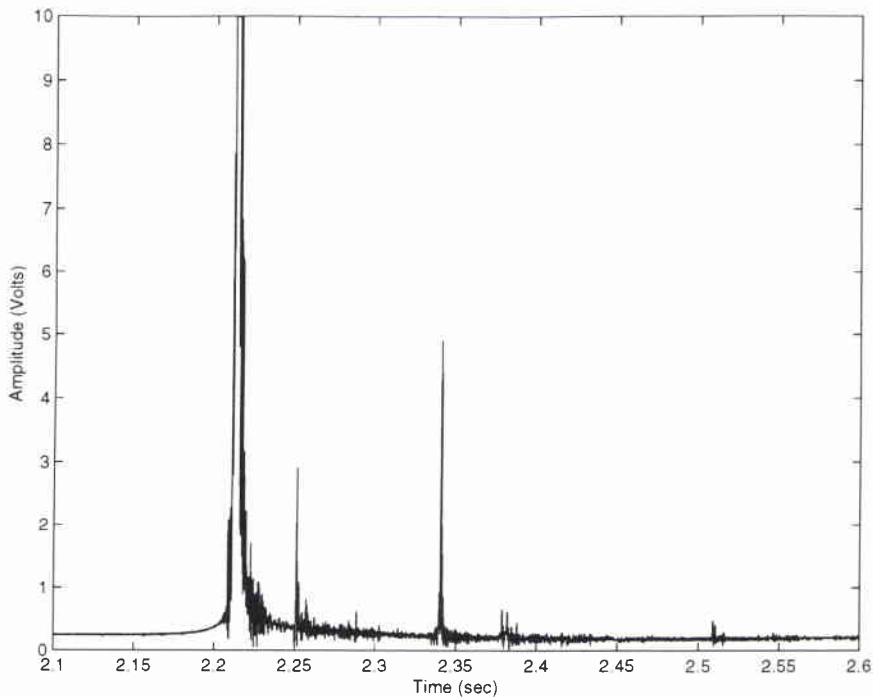
Figure 12 *Hilbert transform of data from top phone. Implosion is at about 2.21 seconds (clipped), bottom arrival is at 2.25 seconds, and surface arrival is at 2.34 seconds*

4

Measurements, environment description, and modeling results

Results from the measurement technique are provided in this section with interpretation based on auxiliary acoustic and geoacoustic measurements. Auxiliary geoacoustic measurements were conducted in order to explore the relationship between bottom scattering and the physical properties of the bottom. This exploration consists of at least two parts, the first of which is the identification of the scattering mechanism(s) and the second part is the determination of the simplest set of physical properties that are required to describe the observations. Following Holland and Neumann (1998), results from bottom reflection measurements are employed to extract key deterministic geoacoustic properties.

4.1 Site 2

Figure 1 shows the bathymetry at Site 2 (water depth of 150 m). The bottom was flat in the north-south direction with a very small (approximately 0.1°) slope in the east-west direction. Sound speed data from a conductivity-temperature-pressure (CTD) cast are shown in Fig. 11a. One of the most crucial parameters required for understanding the dominant scattering mechanism is the sediment sound speed profile (see Holland and Neumann (1998)). Figure 13 shows a high resolution sediment sound speed profile at this site (Holland and Osler (1999)). As confirmed by core data, the upper 50 m are a very soft silty clay (porosity of 80% at the water sediment interface) with very low sound speed and density, about 1470 m/s and 1.33 g/cc respectively at the interface and large positive gradients in both velocity and density. Below this there are randomly interspersed intercalating high speed layers with weak velocity and density gradients between layers.

Seismic reflection data across the scattering area are shown in Fig. 14. The actual scattering experiment took place in a small region, of order several hundred meters around the center of this track. These data serve to indicate that the layering structure is continuous across the region in a large scale sense. The microstructure of the layering is of course discontinuous.

What feature(s) of the bottom is expected to give rise to the scattering? From the sediment sound speed profile and bathymetry, one would expect that scattering from the water-sediment interface would be negligibly small. That is, both the interface impedance contrast and the roughness are small. This is also evident in side scan data from this area which are featureless with occasional faint lines from bottom trawling.

SACLANTCEN SM-364
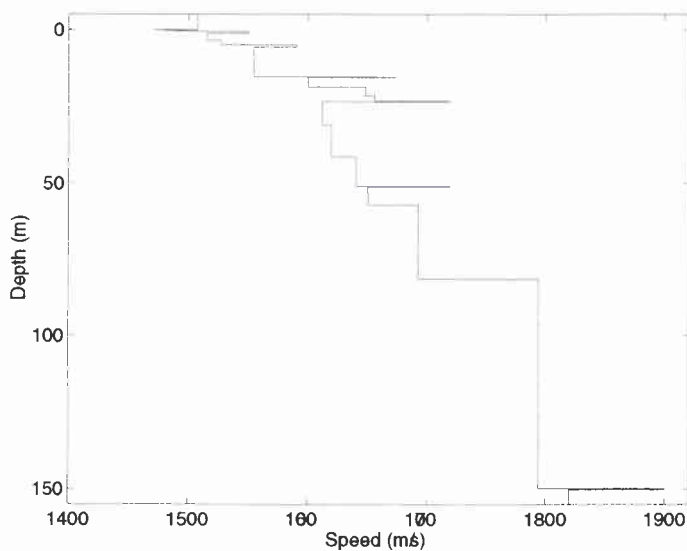
Figure 13 *Sediment sound speed profile at site 2. Note the high speed intercalating layers which are hypothesized to give rise to the sub-bottom scattering.*
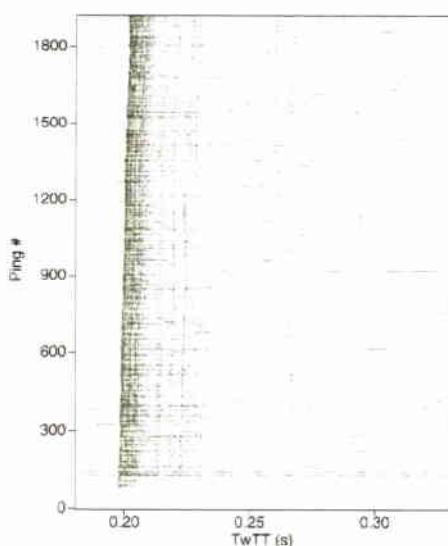
Figure 14 *Seismic data along a 7.5 km track centered at the bottom scattering experiment location.*

Scattering from a sub-bottom basement horizon can also be ruled out, since there was no basement observed within 150 m of the water-sediment interface. Therefore, the most likely geologic feature to give rise to the scattering is the thin high speed layers (i.e., the

– 17 –

sound speed 'spikes' in Fig. 13). Short (1 m barrel) gravity and long (8 m barrel) piston core data indicate at least the first two 'spikes' are sandy silt layers with large shells and coral debris containing fragments as large as 6 m by 6 m. The photograph in Fig. 15, shows the sandy shelly layers at about 0.3^5 and 5 m sub-bottom.

Figure16 shows the measured data at 1800 Hz and 3600 Hz using the ITC array at a source receiver depth of 130 m and 126 m respectively. Note that the SNR is quite good and that there is no evidence of any scattering from biologics from within the water column. The surface reflection is observed through all beams at about 0.17 sec. The hybrid paths (paths b, c, and d in Fig. 2) in the lower beams are substantially lower level than the monostatic path, due the effect of the beampattern in the source and receiver. The relationship between time and angle at the water-sediment interface is shown in Fig. B2.

In order to demonstrate the effect of various scattering mechanisms, some modeling results are presented (a brief description of the model is found in Annex C). The model can be used also to extract quantitative physical sediment properties from the measurements, but at this stage of analysis the primary consideration is to explore the utility and limitations of the measurement technique. The model treats the sediment as a single refracting layer. The modeled sound speed profile in the upper 30 m is shown in Fig. 17.

In order to examine the details of the monostatic arrival branch, the data and model results are shown together in Fig. 18. Measurement results at 1800 Hz and 3600 Hz are shown in Figs. 18a and 18b respectively. Corresponding model results presented in Fig. 18c and 18d predict the scattered field for interface scattering only. Overall, the model shows similar trends as the measured data (the model does not include the direct blast and the surface reflection). There are several useful points to note in the comparison of the model with the data. First, the model-to-data comparison can be used to discern if interface scattering adequately explains the data. At 3600 Hz, the predicted beam spread (Fig. 18d), or width of the monostatic path a, is similar to that observed in the data (Fig. 18b). This result indicates that the scattering at 3600 Hz occurs in the upper approximately 10 m of the seabed.

---

[5] Based on the position of the sandy shelly layer observed in the less disturbed 1 m gravity core, it is presumed that the upper 0.2 meters of the piston core have been lost and/or compacted.

SACLANTCEN SM-364
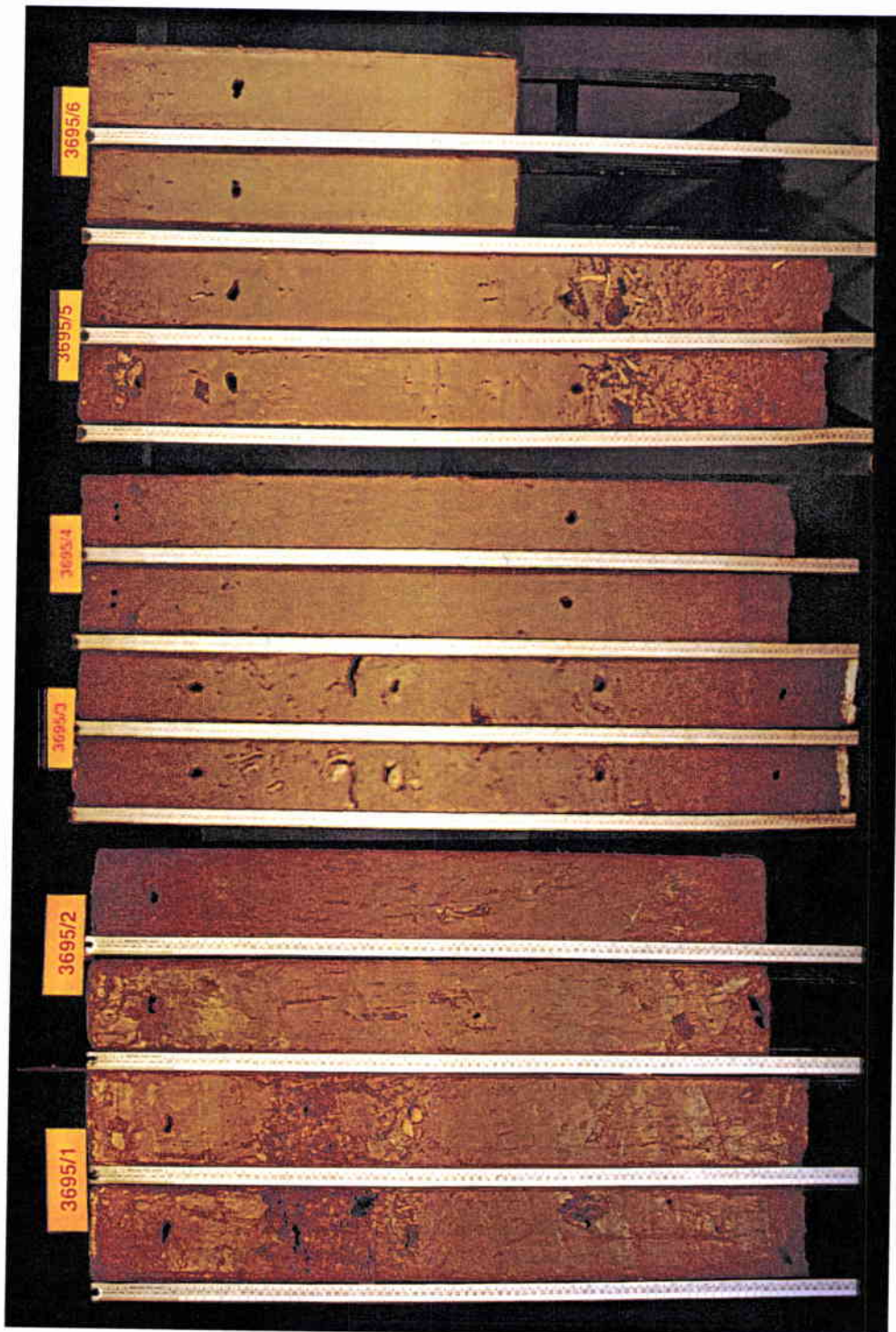
Figure 15 *Photograph of core (uncorrected for compression due to the piston). The core has been sliced down the middle and opened so that each section appears as a pair. Note shells found in layers at 0.30 m and 4.75 m The core from top to bottom (left to right in photograph) is sectioned at 0.85m, 0.81m, 0.90m, 0.83m, 1.06m and 0.60m.*
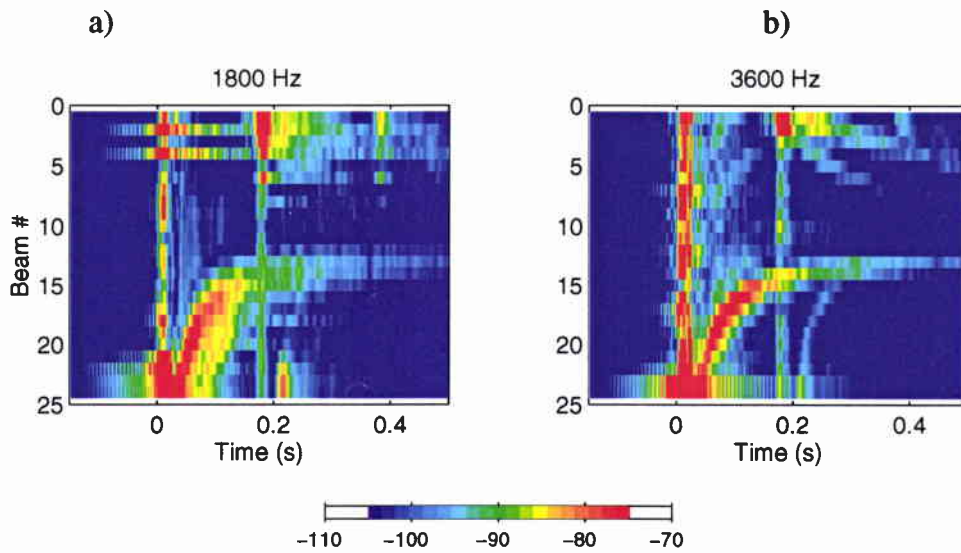
Figure *16 Measured beam time series (10 averages) at Site 2 using two sources at a) 1800 Hz and b) 3600 Hz. The quantity plotted is received level minus source level in dB*
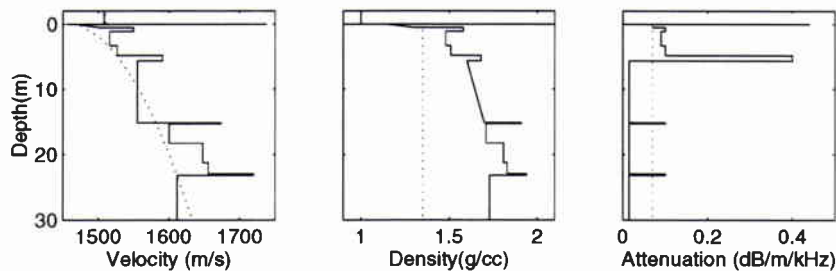
Figure 17 *Site 2 sediment parameters. Parameters from Holland and Osler (1998) (solid line) and that used in the model predictions of Figure 18 (dotted line).*

However, at 1800 Hz (Fig. 18a), it is apparent that there is a later scattering arrival (starting at 0.08 sec in the highest/steepest beam), not seen in the modeled result (Fig. 18c). This late arrival must correspond to a scattering horizon at about 25 m below the water-sediment interface. The sound speed inversion results (Fig. 17) in fact show a high speed layer[1] at 23 m depth in the sediment which is presumed to give rise to the observed phenomenon, based on travel time considerations.

---

[1] The layer is also observed in the seismic data of Fig. 14, and may be of similar constituency as the shelly sand layers observed at 0.5 and 5 meters depth.

SACLANTCEN SM-364
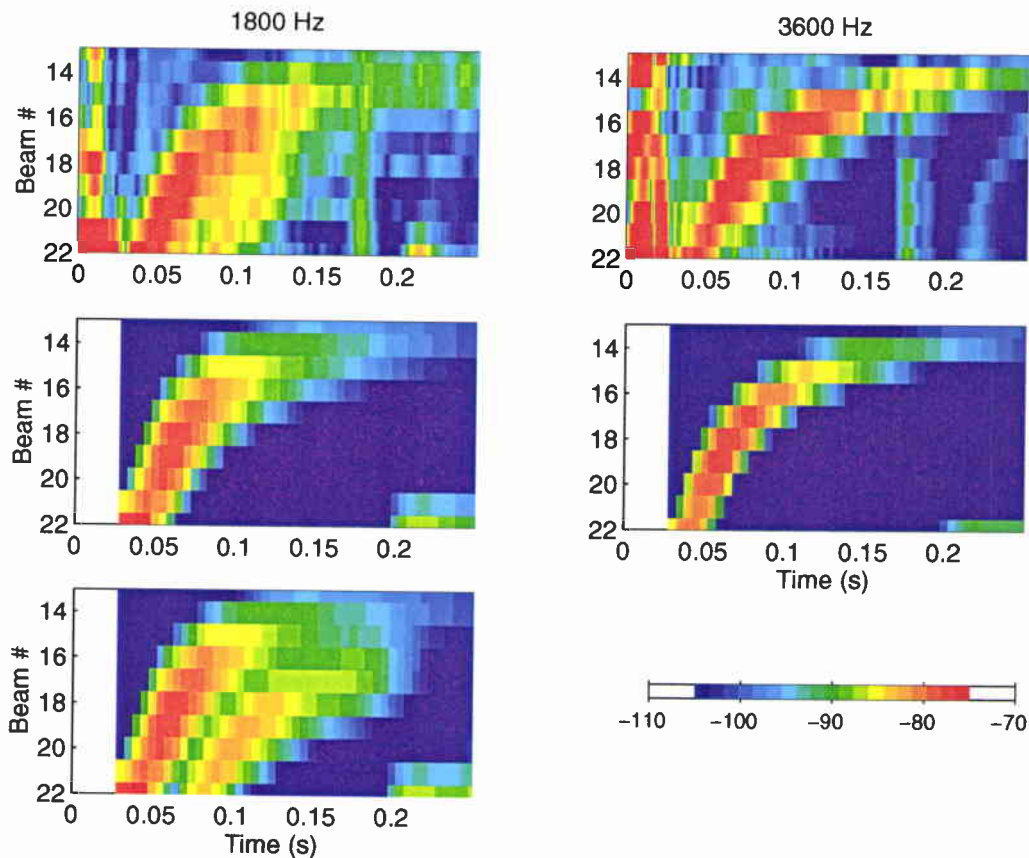
Figure 18 *Comparison of measured data at: a) 1800 Hz and b) 3600 Hz with modeled results for water-sediment interface scattering c) 1800 Hz, d) 3600 Hz and e) 1800 Hz modeled results with both water-sediment interface scattering and interface scattering at 25 m sub-bottom. The lettering sequence follows a left to right, top to bottom order.*

Figure 18e shows model predictions at 1800 Hz including this deeper layer, which in comparison with the measurements in Fig. 18a appears to confirm its existence and general features. There are several differences between the model predictions and the observations that provide further clues about the nature of the scattering. First, the model shows a time separation between the scattering from each interface, whereas the measured data does not. This is interpreted as further evidence that the scattering along the monostatic branch is not interface scattering at all but most probably arises from the shelly sand layers at about 0.5 and 5 m The second difference is that the measured sub-bottom scattering arrival at 1800 Hz decays more rapidly with time than does the modeled result. This could be due to inaccurate assumptions about the angular dependence of the scattering function or due to a rapidly changing transmission coefficient with angle, e.g., due to a critical angle. The latter seems more likely, since the model predictions do not treat the layering structure, e.g., at 0.5 and 5 m sub-bottom. Scattering from the sub-bottom layer at 23 m is not observed at 3600 Hz (Fig. 17b) presumably due to increased attenuation and/or reduced transmissivity through the overlying sedimentary layers.

Scattering strength results are shown in Fig. 19. Detailed analyses of these data will be undertaken at a later time. Rather, it is the intent here to present the data, and provide some observations on the frequency and angular dependencies. Site 2 bottom scattering strength data (red curve) are strongly dependent upon frequency. The monotonically increasing frequency dependence is perhaps due to the fact that the mean scatterer (sub-bottom shell and coral fragments) dimensions are smaller than a wavelength. The observed angular dependence is flatter than Lambert's law, particularly below 3600 Hz; this may also be due to sub-bottom scattering. Various authors (e.g., Novarini and Caruthers (1998), Holland and Neumann (1998)) have shown flatter than Lambert's Law angular dependence in model and/or data results associated with sub-bottom scattering. However, the angular dependence of the observed scattering will depend heavily on the scattering kernel, the sediment sound speed profile between the water-sediment interface and the scatterers, and the source/receiver beam pattern[1]. Overall scattering strengths are less than or equal to the coefficient used by Mackenzie (1961) whose oft-cited frequency independent measurements were conducted in a deep water silty-clay environment
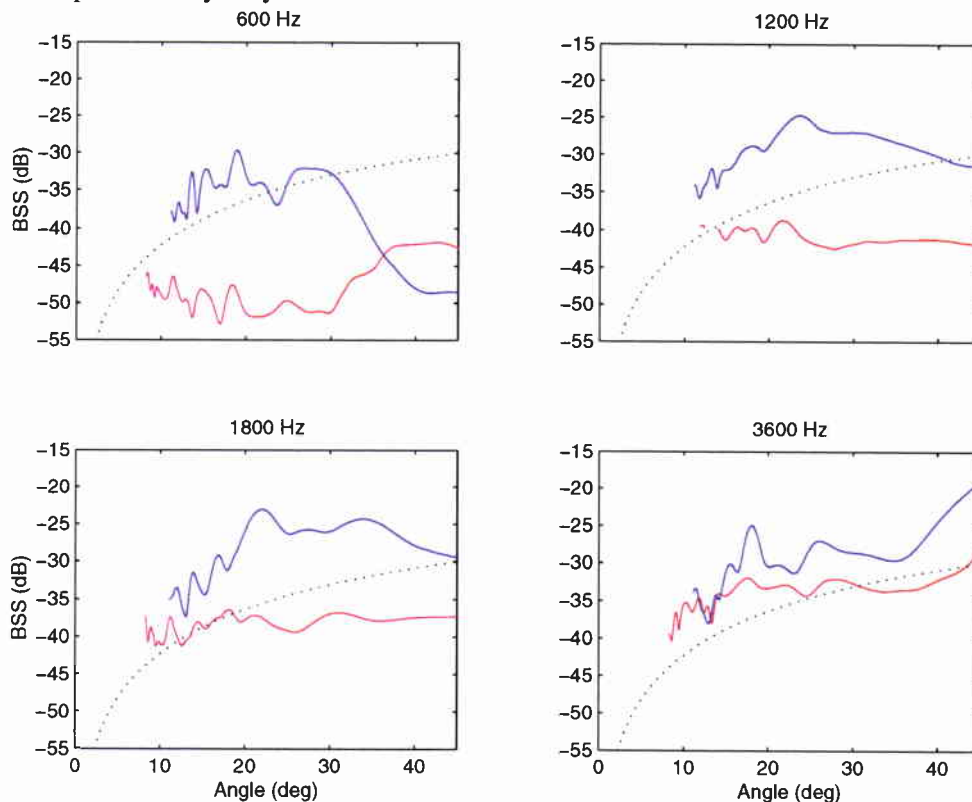
Figure 18 *Comparison of measured data at: a) 1800 Hz and b) 3600 Hz with modeled results for water-sediment interface scattering c) 1800 Hz, d) 3600 Hz and e) 1800 Hz modeled results with both water-sediment interface scattering and interface scattering at 25 m sub-bottom. The lettering sequence follows a left to right, top to bottom order.*

[1] Holland and Neumann (1998) showed that processing artifacts could artificially flatten the angular dependence when the scattering arises from the sub-bottom. This happens because while the processing generally corrects for the beam pattern at the water sediment interface, the scattering actually arises from higher (i.e., less beam loss in this experiment) angles.

4.2 Site 3

The bathymetry showed a small (approximately 0.5°) slope in the east-west direction. Water depth at the scattering experiment location was 104 m Sound speed data from a conductivity-temperature-pressure (CTD) cast are shown in Fig. 11b.

Wide angle reflection measurements at this site are shown in Fig. 20. From these measurements interval velocity and thickness for each layer can be extracted based on the separation and shape of each arrival (see Holland and Osler (1999) for details on experiment geometry and processing). Analyses of these data indicated a 15 m layer with an interval velocity of 1700 and a 5 m layer with a 2100 m/s interval velocity. A 30 m core was collected at this site. Granulometry analyses indicated a fine sand with shell fragments throughout the core. Core sound speed measurements ranged from 1580-1600 m/s.
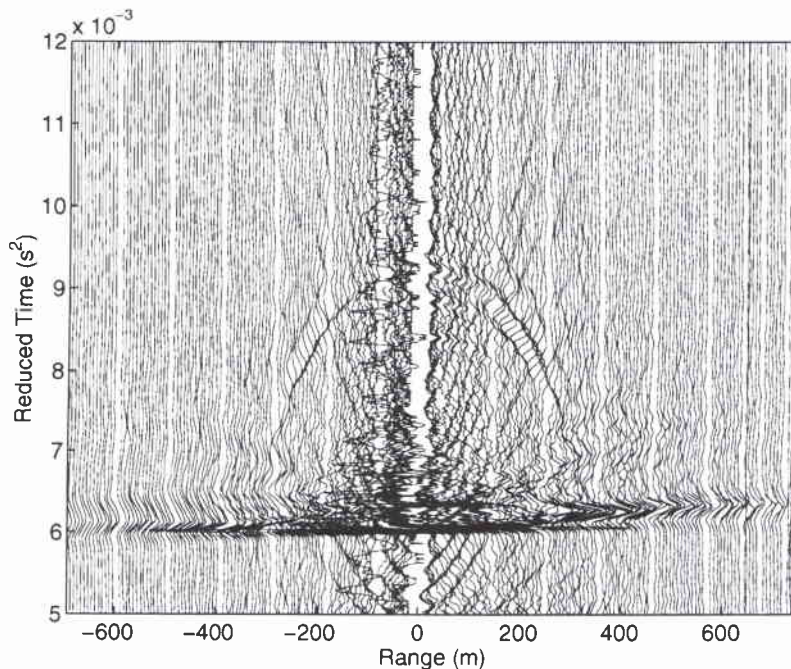
Figure 20 *Wide angle reflection measurements at Site 2. A reducing velocity has been applied to the data to flatten out the arrival structure. At sezo offset the water-sediment interface reflection is observed at 6 s² and the base of the 15m sand layer at 9 s².*
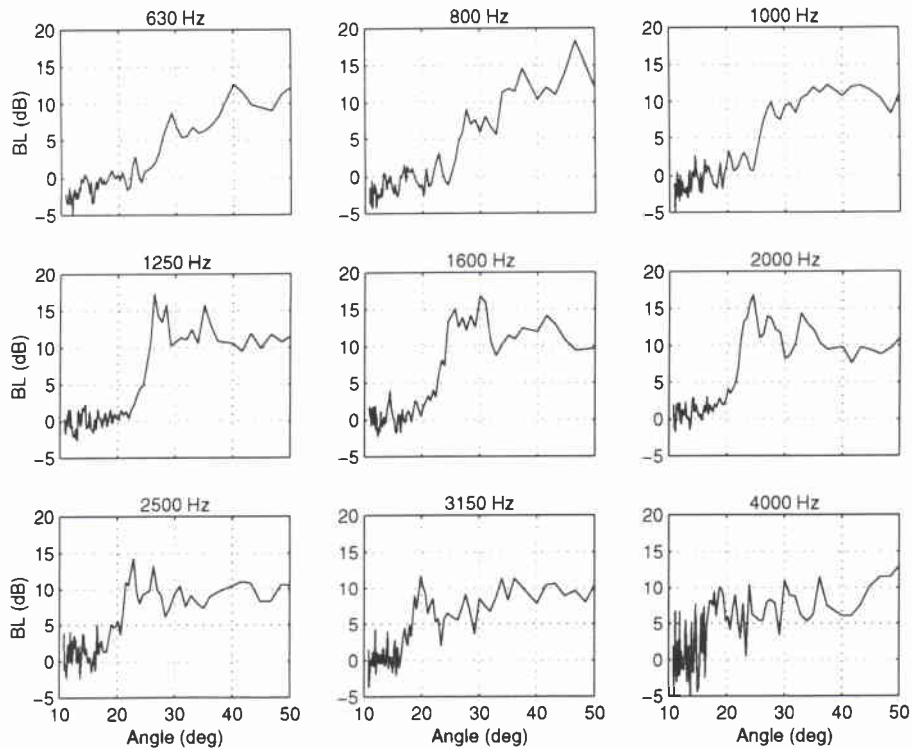
Figure 21 *Measured bottom reflection loss at Site 3.*

Figure 21 shows the bottom reflection loss data at this site. The salient feature of these data is the frequency dependence of the critical angle which is a function of the sound speed profile and attenuation in the bottom. At the highest frequency where a critical angle can be discerned (3150 Hz), the critical angle indicates an effective velocity of 1571 m/s, which compares very favorably to the core measurements in the upper 15 cm. At lower frequencies the observed critical angle increases, i.e., the effective velocity increases. At 1250 Hz the effective velocity is about 1630 m/s (critical angle of 22°) and at 600 Hz the effective velocity is about 1665 m/s (critical angle of 25°). A single layer geoacoustic model (see dotted line Fig. 22) was constructed based on the core data, the interval velocity data, and the frequency dependence of the critical angle. The agreement with the measured data in Fig. 23 is reasonable, but the model does not predict the sharp rise in loss for example at 2000 Hz near 22°. A two layer model (see solid line Fig. 22) was developed that matched the measured reflection loss in Fig. 23 more closely.
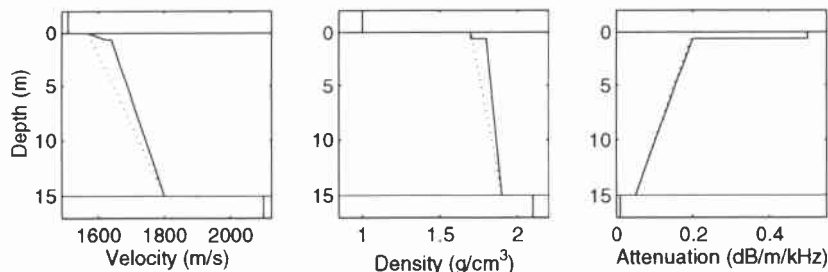
Figure 22 *Geoacoustic models at site 3; 1 layer model (dotted line), two layer model (solid line).*
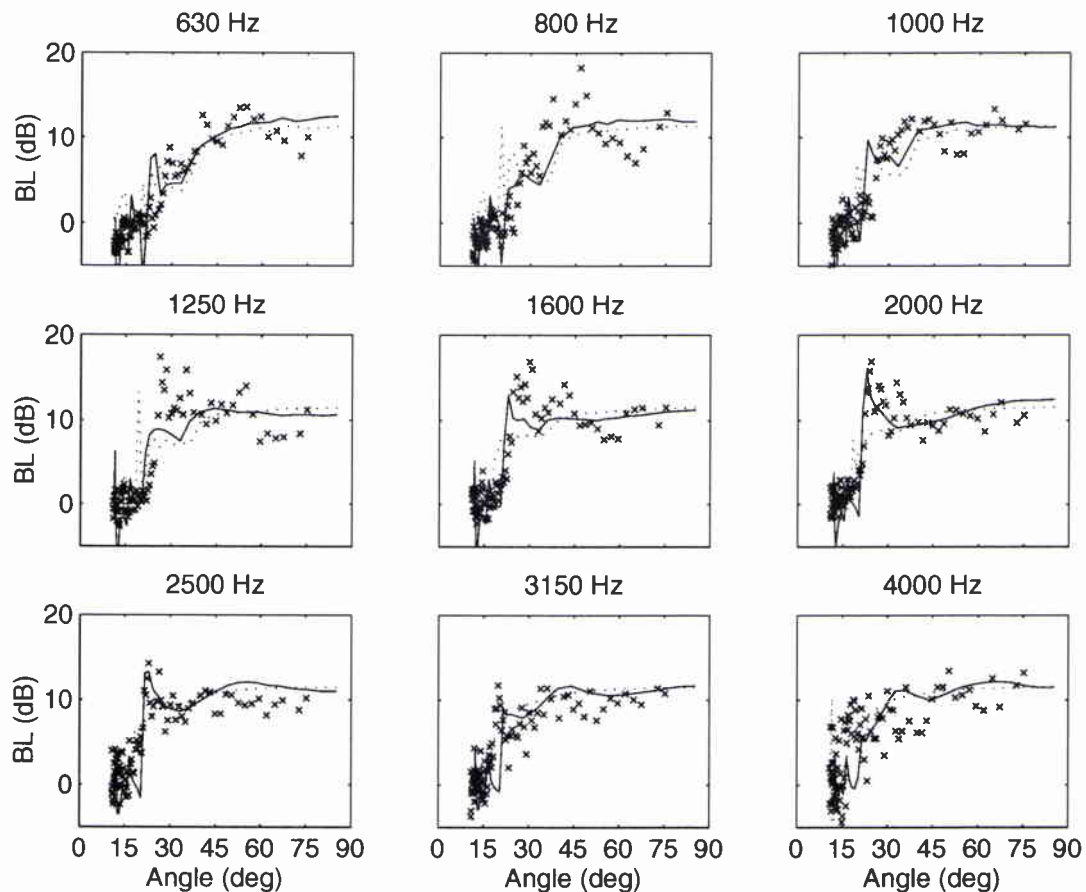
Figure 23 *Measured (*) bottom reflection loss at Site 3 with model predictions from 1 layer model (dotted) and 2 layer sediment model (solid).*

Figure 24 shows the measured data at 1800 Hz and 3600 Hz using the ITC array at a source receiver depth of 79 m and 75 m respectively. The surface reflection is observed through all beams at about 0.10 sec. As with Site 2, there is no evidence of scattering from biologics in the water column. The relationship between time and angle at the water-sediment interface is shown in Fig. B2.

The measured monostatic bottom scattering branch is shown in more detail in Fig. 25a,b at 1800 Hz and 3600 Hz. Model results presented in Fig. 25c,d predict the scattered field for interface scattering. Overall, the model results show similar trends as the measured data. At 1800 Hz and 3600 Hz, the predicted beam spread (or width of the monostatic path a) is similar to that observed in the data. This indicates that the scattering arises from within approximately the first 10 m of sediment.
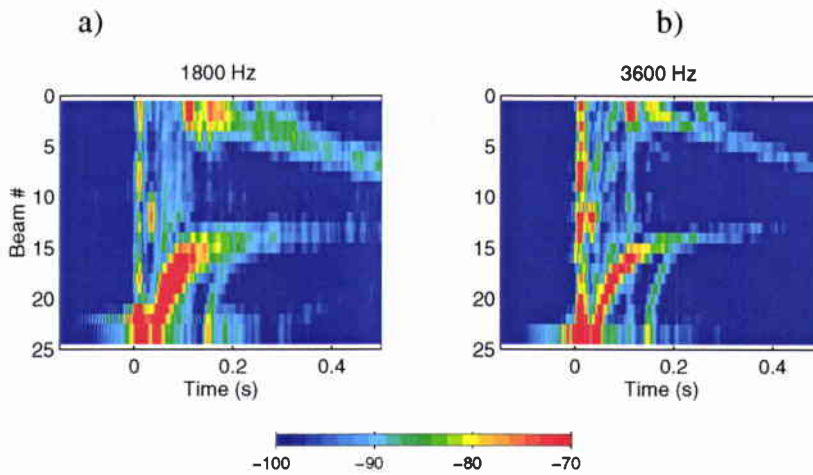
Figure 24 *Site 3 beam time series (10 averages) using two sources at a) 1800 Hz and b) 3600 Hz. The quantity plotted is received level minus source level in dB.*
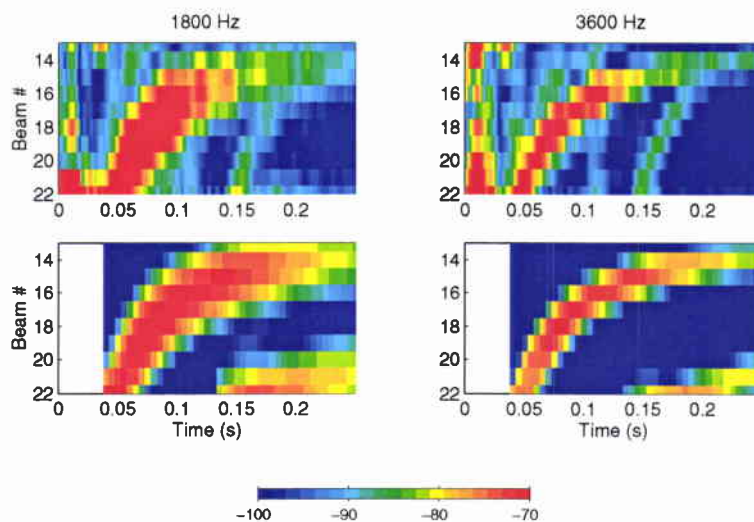
Figure 25 *Site 3 beam measured time series and model results for water-sediment interface scattering only c) 1800 and d) 3600 Hz. The lettering sequence follows a left to right, top to bottom order.*

Scattering strength results at Site 3 shown in Fig. 19 (blue curve) are roughly independent of frequency below 20° grazing angle and substantially larger than at Site 2 for frequencies below 3600 Hz. Frequency independent scattering is consistent with interface scattering theory for a power spectrum of exponent 2. Below 3600 Hz, the angular dependence is similar to Lambert's Law at low angles but changes slope at intermediate angles. For example at 1200 Hz, the slope of the scattering strength changes at 22°. The bottom loss data in Fig. 21 show that at 1200 Hz, there is a critical angle at 22°. A similar slope change and correlation with critical angles can be observed at 1800 Hz and 600 Hz. It may be that the change of slope in the scattering strength is due to a change of mechanism from interface scattering at low angles to sub-bottom volume scattering at intermediate angles.

5

Summary and conclusions

A direct path shallow water bottom scattering measurement technique has been presented. This technique appears to be a useful method for measuring the frequency and angular dependence of bottom scattering. Moreover, the technique can be used to explore the bottom scattering mechanisms. Two data sets were presented. In the first, sub-bottom scattering (25 m sub-bottom) was clearly observable at 1800 Hz. At 3600 Hz, no contribution from 25 m sub-bottom was directly observable, however, the environmental data indicated that scattering from layering down to 5 m sub-bottom dominated the response. For the second site, the scattering appeared to come from at or near the water-sediment interface.

It is important to determine the scattering mechanism in order for physically-based parameters to be extracted. Furthermore, it appears that the scattering mechanism might be related to the statistical characteristics of reverberation. Abraham and Holland (1998) showed that the low frequency reverberation around Site 2 (sub-bottom scattering) was dominated by Rayleigh statistics, while the statistics at Site 2 (interface scattering) were strongly non-Rayleigh.

Future work will focus on techniques for extracting quantitative stochastic sediment properties from these measurements. Also, the technique will be used to validate inversion techniques commonly employed to extract shallow water scattering strength from reverberation measurements.

SACLANTCEN SM-364

Acknowledgments

SACLANTCEN SM-364

References

Abraham, D.A., Holland, C.W. Statistical analysis of low-frequency active sonar reverberation in shallow water, in Proceedings of the Fourth European Conference on Underwater Acoustics, CNR-IDAC, Rome, Ed Alippi and Cannelli, 95-100, 1998.

Blanc, S., Novarini, J.C., Nunez, A.L. Bottom reverberation-derive scattering strengths in shallow water off the Argentinian coast, *Journal of the Acoustical Society of America*, **63**, 1978.

Chapman, R.P., Harris, J.H. Surface backscattering strengths measured with explosive sources, *Journal of the Acoustical Society of America*, **34**, 1962:1592-1597.

Cole, B.F. Podeswa, E.M. Shallow water reverberation under downward refraction conditions, *Journal of the Acoustical Society of America*, **56**, 1974:374-377.

Cable, P.G., Frech, K.D.; O'Connor, J.C.; Steele, J.M. Reverberation-derived shallow-water bottom scattering strength, *IEEE Journal of Oceanic Engineering*, **22**, 1997:534-540.

Ellis, D.D. A shallow water normal mode reverberation model. *Journal of the Acoustical Society of America*, **97**, 1995:2804-2814.

Heard, G.J., McDonald, M., Chapman, N.R., Jashke, L. Underwater lightbulb implosions: a useful acoustic source, Proc. IEEE Oceans '97, 1997.

Holland, C.W., Osler, J. High resolution geoacoustic inversion in shallow water: A joint time and frequency domain technique, SACLANTCEN Report SM-361, 1998.

Holland, C.W., Neumann, P. and sub-bottom scattering: A modeling approach, *Journal of the Acoustical Society of America*, **104**, 1998:1363-1373.

Jackson, D.R., Winebrenner, D.P. Application of the composite roughness model to high frequency bottom backscattering, *Journal of the Acoustical Society of America*, **79**, 1986:1410-1422.

Mackenzie, K.V., Bottom reverberation for 530 and 1030 cps Sound in deep water, *Journal of the Acoustical Society of America*, **33**, 1961:1498-1504.

McDonald, B.E. Holland, C.W. Decay of large underwater bubble oscillations, *Journal of the Acoustical Society of America*, in press.

Mourad, P.D., Jackson, D.R. A model/data comparison for low frequency bottom backscatter, *Journal of the Acoustical Society of America*, **94**, 1996:344-358.

Novarini, J.C., Caruthers, J. A Simplified approach to backscattering from a rough seafloor with sediment inhomogeneities, *IEEE Journal of Oceanic Engineering*, **23**, 1998:157-166.

Scanlon, G.A., Bourke, R.H., Wilson, J.H. Estimation of bottom scattering strength from measured and modeled mid-frequency sonar reverberation levels, *IEEE Journal of Oceanic Engineering*, **21**, 1996:440-450.

Spofford, C.W. The estimation of geoacoustic ocean sediment parameters from measured bottom-loss data, SAIC Technical Report 83-879-WA, McLean, VA (1983).

Sylva, P., Menard, P., Ro, D. A reconfigurable real-time interpolation beamformer,

Zhuo, J., Dinghua, G. Erchang, S., Ensheng, L. Long range reverberation and bottom scattering strength in shallow water, *Chinese Journal of Acoustics*, **1**, 1982:54-63.

Annex A: Source calibration

Calibration measurements were conducted on each of the source arrays using the geometry shown in Fig. A1 from a small workboat. The source array was placed at approximately 11 m below the surface and rotated in the horizontal plane by a stepper motor at 2.59°/sec. Pulses of 15 ms duration were transmitted with a repetition rate of 0.863 Hz; yielding one sample every 3°. The receiver, a B&K8101 hydrophone, was also set at a depth of approximately 11 m. The distance between the source and receiver was measured based on travel time for each deployment but was nominally 5 m

The connectors used for the 2.5 m segments holding the source array were not completely rigid, thus there was some play in the system: of order a few degrees. The effect of this play was minimized by rotating at a constant speed and checked by conducting the rotation in two directions. It was not possible to determine the orientation of the array relative to the receiver with any precision. Thus, the peaks of the theoretical beampattern were used to fix the measurements in absolute angle.
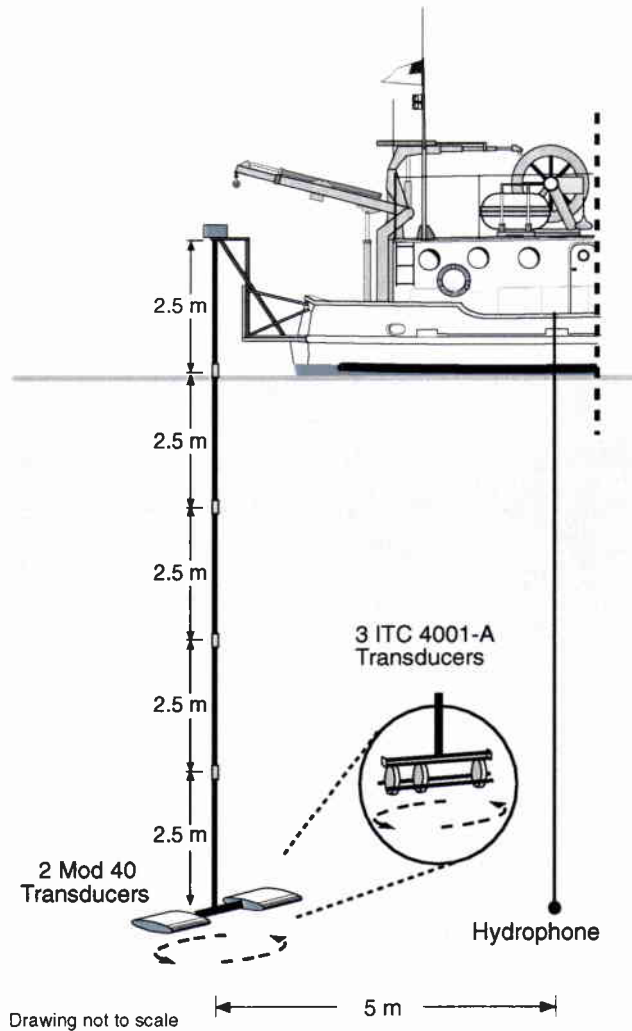
Figure A1. *Experimental set-up for beampattern measurements. The source rotation (i.e.,measurement) plane is in the horizontal.*

The data were peak level processed using a window from 10 to 14 ms which eliminated contamination from source turn-on/turn-off transients and surface path corruption at about 15 ms after the pulse initiation (see Fig. A2).

In Fig. A3 the beampattern measurements from the Mod40 array are provided at 600 Hz and 800 Hz. The solid line is the theoretical result for two omnidirectional point sources at a distance of 5 m   The overall agreement is excellent except near the nulls. The slight asymmetry observed in the nulls at 600 Hz is due to the fact that the amplitude of the two sources are slightly different.

Figure A4 provides the beampattern measurements and theory from the ITC array at 1200 Hz, 1800 Hz and 3600 Hz. At these frequencies there are substantial differences between the theory and the measurements. Those differences are primarily due to the presence of a third transducer in the array (see sketch in Fig. A1). A secondary effect is that the individual transducers are not omnidirectional. The measured beampatterns in Figs. A3 and A4 were used in the data processing (to extract bottom scattering strength) and in the modeling.
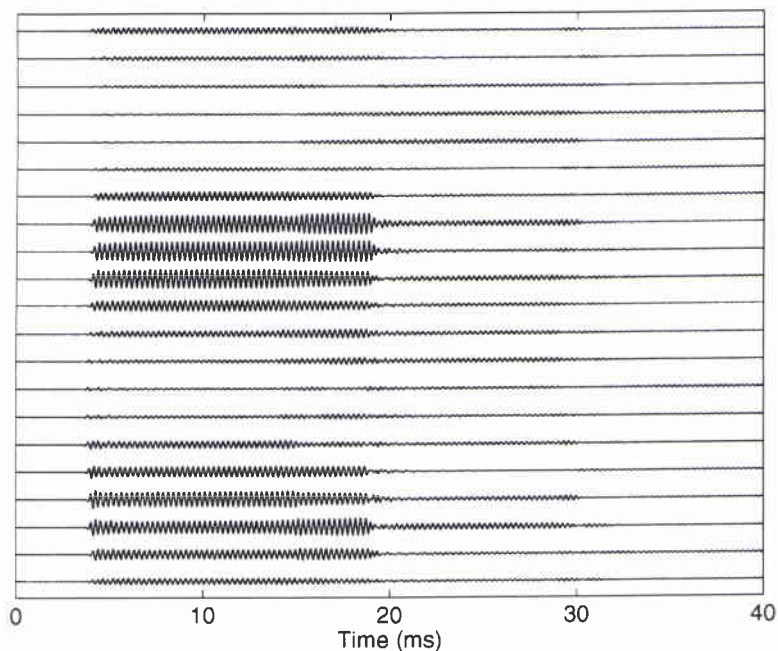
Figure A2. *Raw time series (18 degree increments) from beampattern measurements on ITC array at 3600 Hz. Note surface arrival apparent at about 15 ms.*

a)

b)
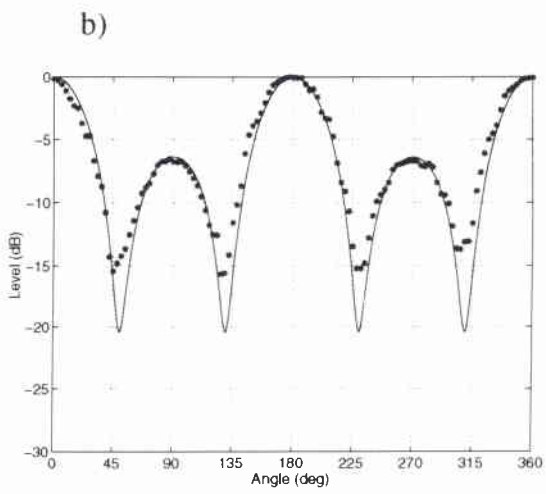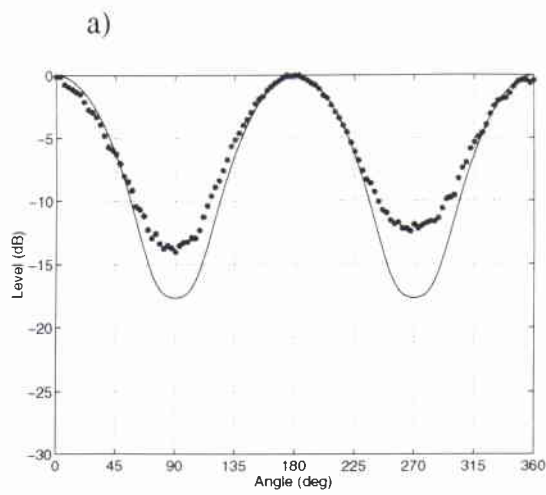
Figure A3. *Beampattern measurements (*) and theory (solid line) for Mod 40 array at a) 600 Hz, b) 800 Hz.*

SACLANTCEN SM-364

a)

b)

c)
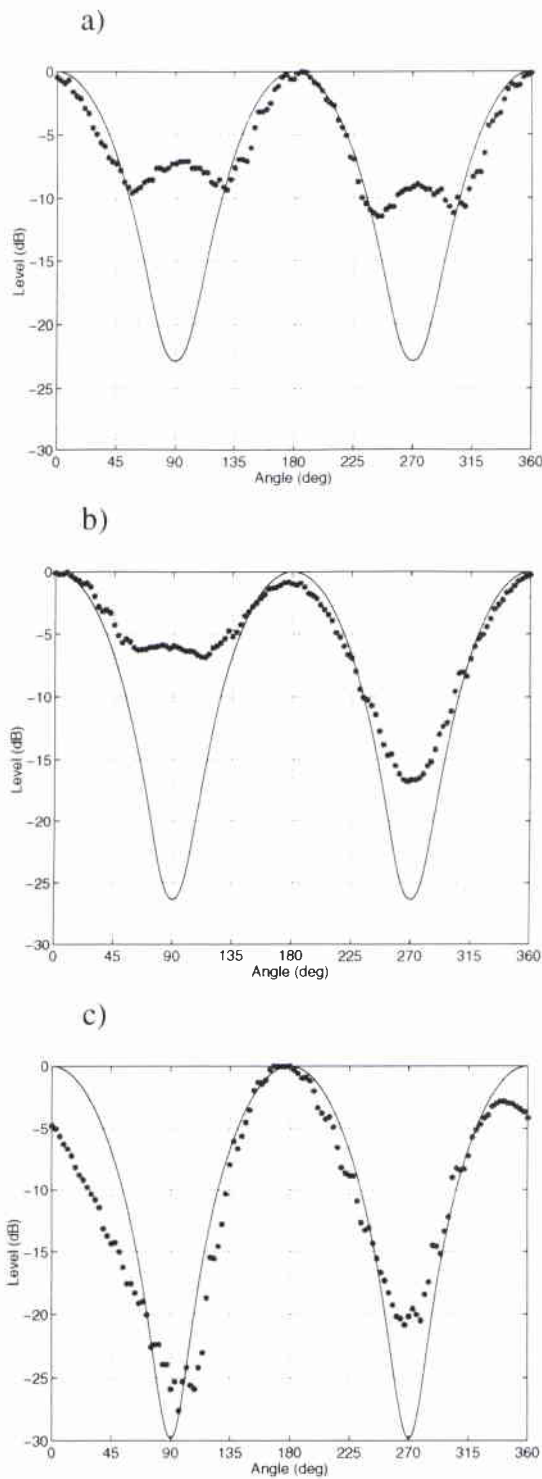
Figure A4. *Beampattern measurements (*) and theory (solid line) for Mod 40 array at a) 1200 Hz, b) 1800 Hz and c) 3600 Hz.*

Annex B: Measurement bi-static angles

Figure B1 shows the difference in incident and scattered angles due to the vertical offset between source and the two receive arrays. Note that the bi-static angle is maximum at 45° and tends toward zero at 0 and 90°. For the results presented in this paper, the reported angle is the angle corresponding to the mean source-receiver height. Figure B2 shows the relationship between time and mean angle for the ITC array at Sites 2 and 3.

The half angle approximation (computing the monostatic scattering strength at the mean of the incident and scattered angles) is valid when the scattering function is linear between the two angles. A Lambert scattering function, for example, is linear around 45°, satisfying the half-angle requirement.
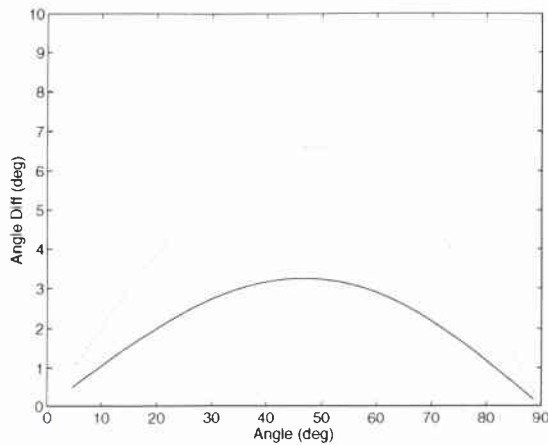
Figure B1 *Difference between incident and scattered angles for the Mod40 source array (dotted) and for the ITC array (solid). Source height is 20 m above the seafloor.*
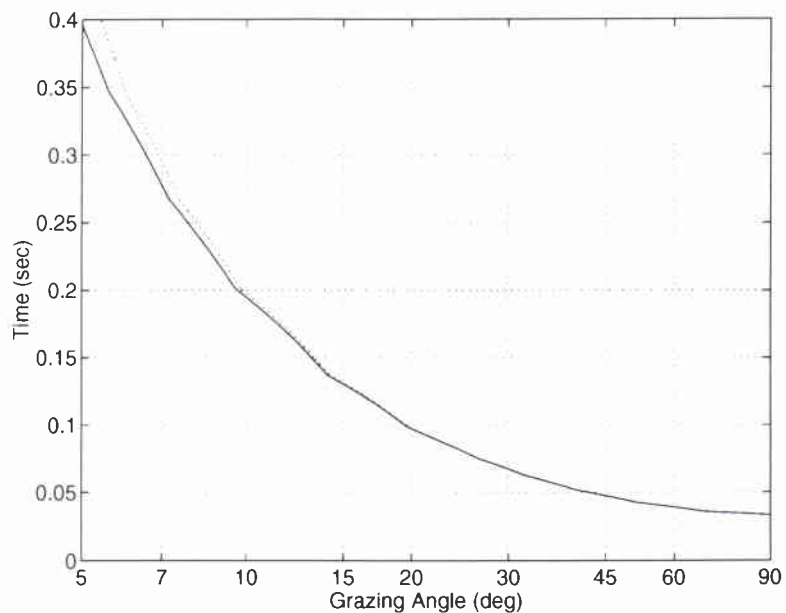
Figure B2. *Relationship between mean grazing angle at water-sediment interface angle and time for geometry at Site 2 (solid line) and Site 3 (dotted line).*

SACLANTCEN SM-364

Annex C: Model for bottom scattering

The modeling approach is described in Holland and Neumann (1998) where for interface scattering the received level is computed on a horizontal grid. For the model used in this study, ray theory was used to compute the TL terms and the grid size was set to 4 m^2. Eigenrays for the direct blast and the normal incidence air-sea reflection were not included in the calculations.

The model allows an arbitrary sound speed profile in the water column, a single refracting fluid sediment layer and a basement halfspace. The form for the sediment sound speed $c(z)$ as follows that proposed by Spofford *et al.* (1983)

$$c(z) = c_o \left[(1 + \beta)(1 + 2g_o z /(c_o(1 + \beta)))^{1/2} - \beta \right] \qquad \text{(C1)}$$

where z is depth in meters, c_o is the speed at the top of the sediment, g_o is the initial gradient and β is a parameter that controls the curvature.

Interface scattering for both the water-sediment interface and the sub-bottom interface was computed using composite roughness theory (Jackson and Winebrenner (1986)). Volume inhomogeneities were not included in the modeling in this phase of the analysis.

Document Data Sheet

Security Classification		Project No.
UNCLASSIFIED		04-C

Document Serial No.	Date of Issue	Total Pages
SM-364	August 1999	41 pp.

Author(s)

Holland, C.W., Hollett, R., Troiano, L.

Title

Bottom scattering measurements in shallow water.

Abstract

Sonar performance predictions of reverberation in shallow water rely upon good estimates of the bottom scattering strength. However, little is understood about bottom scattering in shallow water in the frequency range 400 – 4000 Hz, particularly its dependency upon frequency and its relationship to the physical properties of the seafloor. In order to address these issues, new measurement techniques have been developed to probe the frequency and angular dependency of bottom scattering strength. The measurement techniques also appear to be capable of revealing the physical mechanisms that give rise to the scattering. Several experimental techniques will be described, including use of coherent and incoherent sources (lightbulbs). The general experimental approach is also described which includes auxiliary acoustic and geoacoustic measurements designed to allow exploration of the relationship between bottom scattering and the physical properties of the bottom. Measurement and modeling results for two shallow water sites are presented. At one site, the scattering appeared to arise from at or near the water-sediment interface. At the other site, scattering from a 25 m sub-bottom horizon is clearly apparent in the data at and below 1800 Hz.

Keywords

Issuing Organization

North Atlantic Treaty Organization
SACLANT Undersea Research Centre
Viale San Bartolomeo 400, 19138 La Spezia, Italy

*[From N. America: SACLANTCEN
(New York) APO AE 09613]*

Tel: +39 0187 527 361
Fax:+39 0187 524 600

E-mail: library@saclantc.nato.int